

## ORIGINAL ARTICLE

# *In situ* observations of the mesophase formation of isotactic polypropylene—A fast time-resolved X-ray diffraction study

Koji Nishida<sup>1</sup>, Kazuma Okada<sup>1</sup>, Harutoshi Asakawa<sup>1</sup>, Go Matsuba<sup>1,2</sup>, Kazuki Ito<sup>3</sup>, Toshiji Kanaya<sup>1</sup> and Keisuke Kaji<sup>1</sup>

*In situ* observation of the formation process of a mesophase of isotactic polypropylene is reported from a structural point of view. A very rapid transformation from the molten state to the mesophase has, for many years, made *in situ* observation difficult. In the present study, a rapid temperature jump and high-flux synchrotron radiation X-ray scattering techniques were combined effectively to observe this transformation. Fast time-resolved wide-angle X-ray diffraction during rapid cooling clearly shows the time evolution of the transformation from the molten state to the mesophase. The transformation proceeded very quickly in a narrow temperature range below ca 35 °C. Furthermore, the transformation was accompanied by instantaneous density fluctuations throughout the system, as visualized by microscopic observations. These observations suggest that the mesophase formation proceeds similarly to spinodal decomposition.

*Polymer Journal* (2012) 44, 95–101; doi:10.1038/pj.2011.118; published online 23 November 2011

**Keywords:** isotactic polypropylene (iPP); mesophase; polymer crystallization; rapid temperature jump; spinodal decomposition (SD); SPring-8; wide-angle X-ray diffraction (WAXD)

## INTRODUCTION

Isotactic polypropylene (iPP) has a mesophase,<sup>1,2</sup> in addition to three major crystalline phases, the alpha, beta and gamma forms.<sup>3</sup> The macroscopic appearance of the mesophase iPP is transparent, similar to a glassy polymer.<sup>4</sup> Despite its macroscopic transparency, the mesophase iPP shows hierarchical structures on different microscopic scales. On a crystallographic scale, it has an intermediate structure between amorphous and crystalline, as was characterized by two broad peaks in the wide-angle X-ray diffraction (WAXD) pattern. Specifically, the mesophase iPP has, locally, a liquid crystal-like order.<sup>1,5</sup> On a mesoscopic scale, it shows a dense packing of granular particles, so-called ‘nodules,’ with a diameter of ~10 nm, as observed by transmission electron microscopy<sup>6,7</sup> and atomic force microscopy.<sup>8,9</sup> In reciprocal space, a broad peak due to the nodular structure was observed by small-angle X-ray scattering (SAXS).<sup>7</sup>

The mesophase iPP is obtained by quenching molten amorphous iPP; empirically, this is achieved by dropping a thin piece of a sample rapidly into ice water.<sup>5</sup> During this process, the sample experiences a cooling rate of the order of 100 °C s<sup>-1</sup>. Specifically, the formation speed of the mesophase iPP is particularly high, and the formation process is completed over a short period of time. Extensive *ex situ* analysis of the transformation process to the mesophase of iPP has been performed.<sup>8,10–15</sup> Additionally, the crystallization of iPP via the

mesophase has been extensively studied in the literature.<sup>7,16–21</sup> However, the ongoing process of mesophase formation has been a black box for many years, and *in situ* observation of the formation process, which occurs in a very short period of time, has been challenging.

Initial *in situ* observations were performed by a fast differential scanning calorimetric (fast DSC) technique,<sup>22</sup> and an exothermal shoulder peak due to the mesophase formation was observed. In subsequent studies, an ultra-fast DSC technique successfully resolved two exothermal peaks due to crystallization and the mesophase formation.<sup>23</sup> The exothermal peak due to the mesophase formation is located between ca –20 °C and ca 35 °C, and the amount of the exotherm is comparable to that of crystallization. The lower temperature limit was ascribed to the glass transition temperature,  $T_g$ , of the amorphous phase of iPP.<sup>7,24</sup> Thus, the formation of the mesophase of iPP is one of the solidification processes, which accompanies an exotherm (latent heat) sufficient to stabilize the mesophase at room temperature (above the  $T_g$ ).<sup>21</sup> The understanding of the formation process of the mesophase iPP has progressed significantly as a result of thermal analysis.

From a structural point of view, the first *in situ* observations of mesophase iPP formation were accomplished by heating from the glassy amorphous state, which is the reverse process of quenching

<sup>1</sup>Institute for Chemical Research, Kyoto University, Kyoto, Japan; <sup>2</sup>Department of Polymer Science and Engineering, Graduate School of Science and Engineering, Yamagata University, Yamagata, Japan and <sup>3</sup>RIKEN SPring-8 Center, Harima Institute, The Institute of Physical and Chemical Research (RIKEN), Hyogo, Japan  
Correspondence: Dr K Nishida, Institute for Chemical Research, Kyoto University, Uji, Kyoto 611-0011, Japan.

E-mail: knishida@scl.kyoto-u.ac.jp

Received 31 March 2011; revised 14 September 2011; accepted 16 September 2011; published online 23 November 2011

from the molten amorphous state. Although it requires different techniques to obtain the glassy amorphous iPP rather than the mesophase iPP, the *ex situ* preparation of the former was still possible with an ultra-quenching technique using cold ethanol or isopentane as a cooling medium.<sup>6,7</sup> Once the glassy iPP is obtained below  $T_g$ , the progress of the mesophase formation can be controlled by slow heating. Thus, the development of the two broad peaks in WAXD and the broad peak in SAXS, which are characteristics of the mesophase iPP, were successfully observed.<sup>24</sup> Most recently, by using a propene/ethylene copolymer<sup>25</sup> to effectively delay the formation rate of the mesophase, *in situ* observation of the formation process of the mesophase from the molten state has been achieved.<sup>26</sup> Thus, *in situ* observation of the formation process of mesophase iPP has been challenging.

In the present work, we attempted the *in situ* observation of the formation of the mesophase of an iPP homopolymer by quenching directly from the molten amorphous state. Fast time-resolved WAXD observations during the quenching were accomplished by combining high-flux synchrotron radiation X-ray scattering<sup>27</sup> and a rapid temperature jump technique.<sup>28</sup> As the diffraction profile of a sufficiently grown mesophase of iPP indicates the characteristic profile of two broad peaks, which is a different profile from the one very broad peak observed for the amorphous state, we believe that the present attempt to observe structural developments is promising, assuming that the quenching conditions meet the requirements for mesophase formation and that the time resolution of the X-ray detectors utilized is capable of keeping up with the extremely rapid structural developments.

## EXPERIMENTAL PROCEDURE

### Materials and sample preparations

The iPP material was supplied from Idemitsu Unitech Co., Ltd; the weight-average molecular weight was  $M_w=380\,000$ , with a polydispersity of  $M_w/M_n=4.5$  and a degree of isotacticity (a meso pentad value) of  $mmmm=0.93$ . This isotacticity is greater than the critical value (0.68) of isotacticity required to form the mesophase.<sup>14</sup> Sample films were prepared by quenching molten iPP to 0 °C by dipping them into ice water. For WAXD measurements, 200  $\mu\text{m}$ -thick films were sandwiched between 10  $\mu\text{m}$ -thick aluminum foils.

### Temperature jump stage

We have developed a temperature jump type hot stage consisting of two thermally separated heat blocks.<sup>28</sup> The temperature of each heat block was regulated independently. The sample cells consisted of a spacer rim and a pair of window materials such as aluminum foils for X-ray measurements or glass for optical measurements. Sample cells containing thin films were transferred immediately from one block to the other by passing through flat gaps and arranged colinearly inside the blocks. The thickness of the gap was adjusted to maintain a good thermal contact between the heat block and the sample cell. The heat capacity of the block was designed to be much larger than that of the sample cell so that the sample would approximately experience a relaxation-type temperature variation  $T(t)$  with time  $t$  as

$$T(t) = (T_1 - T_2) \exp(-t/\tau_{\text{cooling}}) + T_2 \quad (1)$$

where  $T_1$ ,  $T_2$  and  $\tau_{\text{cooling}}$  are the temperatures of the first and second heat blocks and the characteristic time of cooling, respectively.  $T(t)$  was monitored by a thin thermocouple attached to the sample cell. Figure 1 shows a typical cooling curve monitored for a case where  $T_1=200$  °C and  $T_2=-10$  °C using 10  $\mu\text{m}$ -thick aluminum foil with the sample cell. This case corresponds to the condition for time-resolved WAXD measurements as is described below (Figure 2a). The open circles represent the observed values, and the solid line is a curve that was fit according to equation (1), where  $\tau_{\text{cooling}}=0.36$  s gives the best fit. The accuracy of  $\tau_{\text{cooling}}$  may be affected by the conditions in the sample

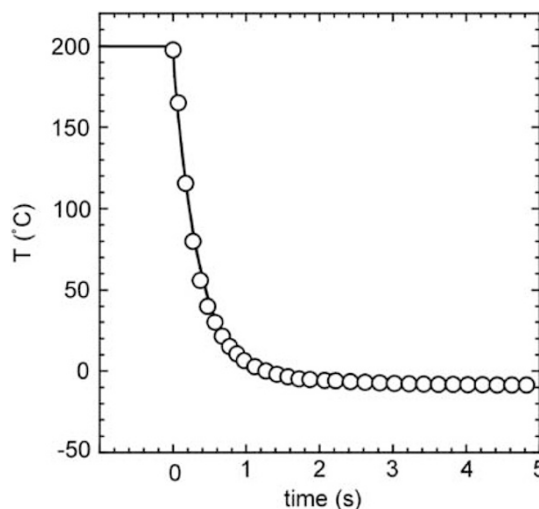


**Figure 1** A typical cooling curve for  $T_1=200$  °C and  $T_2=-10$  °C using 10  $\mu\text{m}$ -thick aluminum as the sample cell (see text).

cell, so the cooling curve was calibrated for each case using the actual measurements of  $T(t)$ .

A commercially available version of this apparatus is available from Japan Hightech and Linkam as LK-300. Further description of the apparatus is available elsewhere.<sup>28</sup>

### WAXD measurements

Fast time-resolved WAXD measurements were conducted using a high-intensity undulator X-ray beam line BL45XU<sup>27</sup> in a synchrotron radiation facility, SPring-8, Hyogo, Japan. In the present measurements, the wavelength of the incident X-ray,  $\lambda$ , was set to 0.9 Å using a double crystal monochromator made of a set of synthetic diamonds to facilitate the transmission in the sample. The scattering vector  $q$  ( $=4\pi \sin \theta/\lambda$ ) was covered from 8 to 18  $\text{nm}^{-1}$  for the WAXD measurements, where  $\theta$  is half the scattering angle ( $2\theta$ ). Scattered X-rays were detected by an image-intensified CCD camera with a capturing frequency 25 Hz at 0.04 s intervals in the fastest case. After standard data processing, such as correcting detector sensitivity and subtracting scattering from the empty sample cell, the WAXD data were circularly averaged because the 2D data showed no anisotropy.

### Optical microscope observations

The time evolution of the optical micrographs was recorded with a Nikon Optiphot2-Pol (Nikon, Tokyo, Japan) with a CCD camera and a video recorder. The bright field mode was used, although the polarized light mode is often used for the observation of polymer crystallization because the mesophase iPP gives only very weak optical retardation. The capturing frequency was 30 Hz according to the NTSC (National Television System Committee) format.

## RESULTS AND DISCUSSION

### Time-resolved WAXD

Fast time-resolved WAXD measurements were carried out while the molten iPP was rapidly cooled to various temperatures of  $T_2$ . Figures 2a–d show typical examples of the time evolution of the WAXD profiles for  $T_2=-10$ , 20, 40 and 80 °C, respectively. For all the  $T_2$ s, the WAXD profile initially shows a single broad peak at  $\sim q=11$   $\text{nm}^{-1}$ , which is characteristic of the molten amorphous state. The subsequent development depends on  $T_2$ . At  $T_2=-10$  °C (Figure 2a), monotonic development of the second broad peak at  $\sim q=15$   $\text{nm}^{-1}$ , which is characteristic of the mesophase iPP, is observed and is similar to the case for heating from the glassy amorphous state.<sup>24</sup> The resultant sample showed a broad SAXS peak at  $\sim q=0.6$   $\text{nm}^{-1}$ , in a preliminary

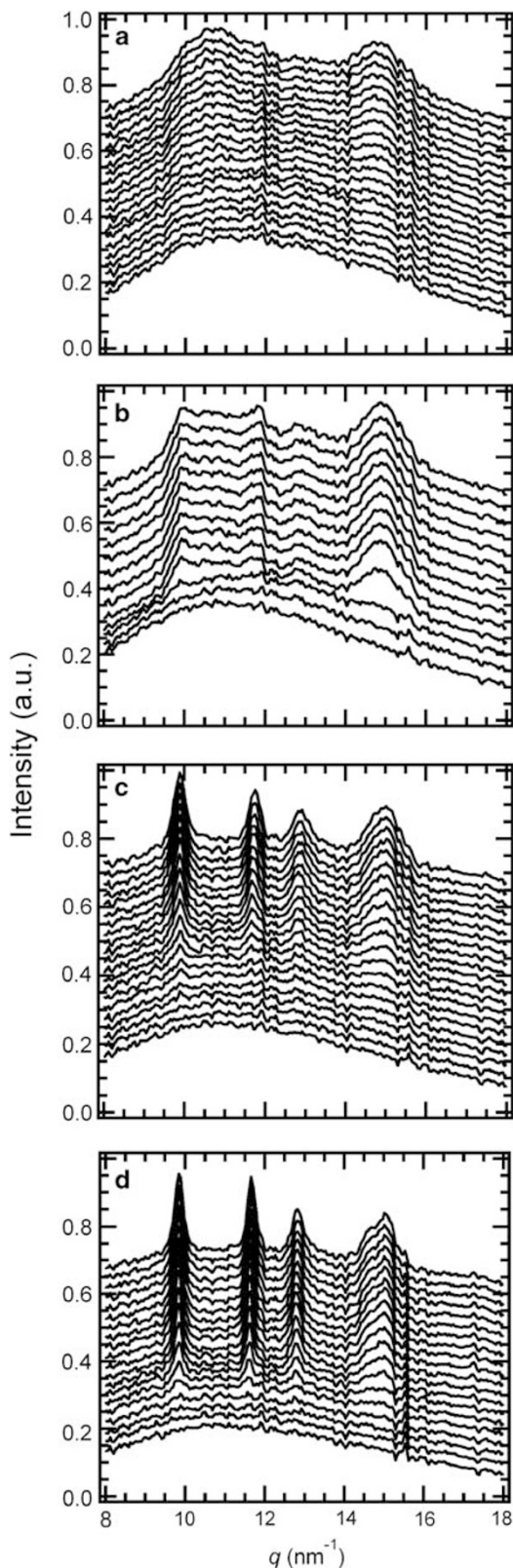


**Figure 2** Time evolution of WAXD profiles during the rapid cooling of molten iPP to temperatures,  $T_2$ . (a)  $T_2 = -10^\circ\text{C}$ , profiles are shown in every 0.04 s from  $t = 0.2$  s to 1.0 s. (b)  $T_2 = 20^\circ\text{C}$ , profiles are shown in every 0.4 s from  $t = 0$  s to 5.2 s. (c)  $T_2 = 40^\circ\text{C}$ , profiles are shown in every 0.08 s from  $t = 0.2$  s to 1.8 s. (d)  $T_2 = 80^\circ\text{C}$ , profiles are shown in every 0.16 s from  $t = 0.2$  s to 3.4 s.

measurement, which is considered to be due to the nodular structure. This value corresponds to ca 10 nm in real space. The broad SAXS is also a characteristic of the mesophase iPP, as mentioned previously.<sup>6–9</sup> Detailed SAXS studies will be reported elsewhere. Inferring from the monotonic development, we believe that no other intermediate state exists between the amorphous and mesophase on a crystallographic scale. Qualitatively, the mesophase iPP fades away with increasing  $T_2$ , while the alpha crystal becomes apparent.

In order to quantify this behavior, the WAXD profiles were separated into three components of alpha crystal, mesophase and amorphous, according to a previously reported method.<sup>14</sup> Here, we leave room for the possibility that the amorphous component includes a nematic phase, which may have been produced just after quenching because their WAXD profiles are considered indistinguishable. Figures 3a–d show examples of the component analyses for the final WAXD profiles at  $T_2 = -10, 20, 40$  and  $80^\circ\text{C}$ , which were shown in Figures 2a–d, respectively. Open circles represent the observed WAXD data, and the thin solid lines, thin dotted lines and thick dotted lines indicate the crystalline, mesophase and amorphous components, respectively. Here, the crystalline and mesophase components are described by the assembly of Lorenz curves. A smoothed curve of the WAXD profile for the molten state is used as a reference curve for the amorphous component. Thick solid lines, which are the summations of the crystalline, mesophase and amorphous components, reproduce the observed WAXD profiles fairly well. The fractions  $\Phi_{\text{cryst}}$ ,  $\Phi_{\text{meso}}$  and  $\Phi_{\text{amorph}}$  of the alpha-crystal, mesophase and amorphous components, respectively, were obtained as the ratios of the integrated intensity of each component to the total integrated intensity. Figure 4 shows such fractions as a function of time,  $t$ , during the rapid cooling process. The conditions in Figures 4a–d correspond to those in Figures 2a–d, respectively. For  $T_2 = -10^\circ\text{C}$  (Figure 4a),  $\Phi_{\text{meso}}$  starts to increase at  $\sim t = 0.5$  s and levels off at  $\sim t = 2.0$  s. In this way, the mesophase formation finishes in a very short time. The time  $t = 0.6$  s corresponds to the temperature  $T = 30^\circ\text{C}$  in Figure 1. This temperature is considered to be around the onset temperature where mesophase formation is favorable. During the cooling process, only the development of  $\Phi_{\text{meso}}$  is observed, and  $\Phi_{\text{cryst}}$  is not detected. At  $T_2 = 20^\circ\text{C}$  (Figure 4b), development of  $\Phi_{\text{meso}}$  is still predominant, but  $\Phi_{\text{cryst}}$  develops somewhat. At  $T_2 \geq 40^\circ\text{C}$  (Figures 4c and d), development of  $\Phi_{\text{meso}}$  is no longer detected, and the development of  $\Phi_{\text{cryst}}$  becomes predominant instead.

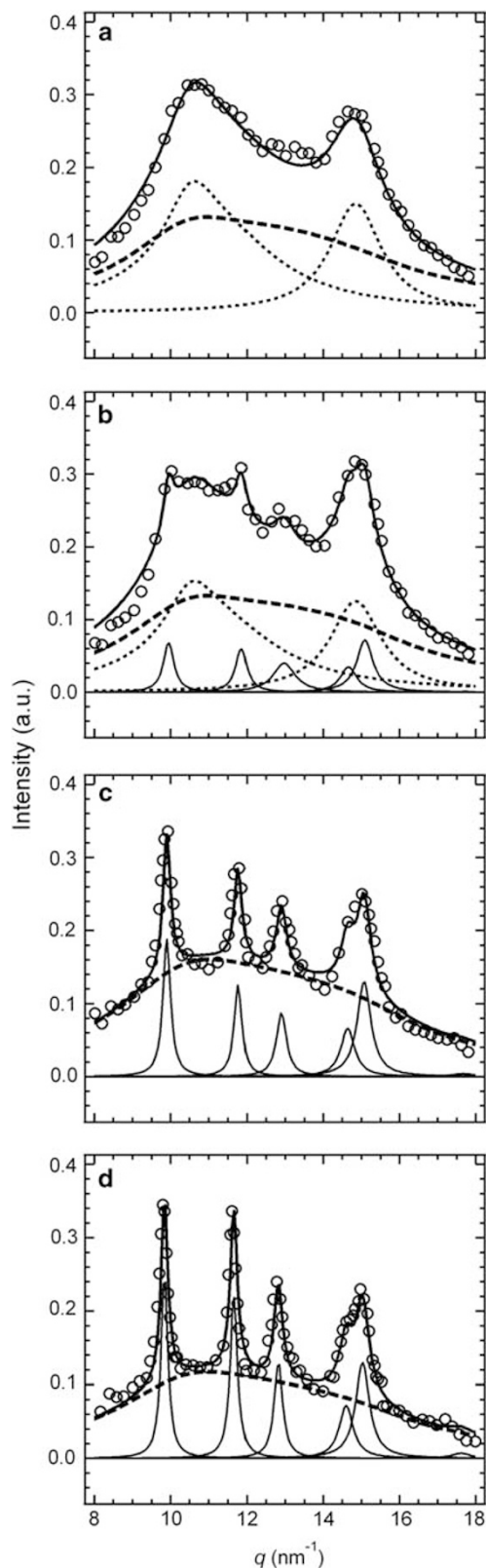
#### Fractions of crystal and mesophase at the final stage of cooling

Figure 5 shows the fractions of alpha-crystal  $\Phi_{\text{cryst}}$  and mesophase  $\Phi_{\text{meso}}$  at the end of cooling as a function of temperature,  $T_2$ .  $\Phi_{\text{cryst}}$  starts to increase gradually with temperature and rather steeply increases between 30 and  $50^\circ\text{C}$ . Meanwhile,  $\Phi_{\text{meso}}$  decreases gradually below  $30^\circ\text{C}$  and drastically between 30 and  $40^\circ\text{C}$ ; it is not detected above  $40^\circ\text{C}$ . Taking these results and the time-resolved WAXD data (Figure 4a) into consideration, we conclude that the most favorable temperature range for mesophase formation is located below  $35 \pm 5^\circ\text{C}$ . This upper crossover temperature, as obtained by the present analysis, is consistent with the value obtained by ultra-fast DSC.<sup>23</sup>

#### Formation rate of the mesophase along a specific path

In the previous sections, the formation of the mesophase iPP was surveyed from a structural viewpoint, and the yield of the mesophase as a function of quenching temperature or the final temperature,  $T_2$ , was obtained as in Figure 5. In the present section, we discuss the kinetics of formation of the mesophase iPP. In general, the transition





**Figure 3** Examples of component analyses. Parts (a–d) correspond to the final WAXD profiles at  $T_2 = -10, 20, 40$  and  $80^\circ\text{C}$ , which were shown in Figures 2a–d, respectively. Open circles, thin solid lines, thin dotted lines and thick dotted lines represent the observed WAXD profiles, crystalline, mesophase and amorphous components, respectively. Thick solid lines represent the fitting curves.

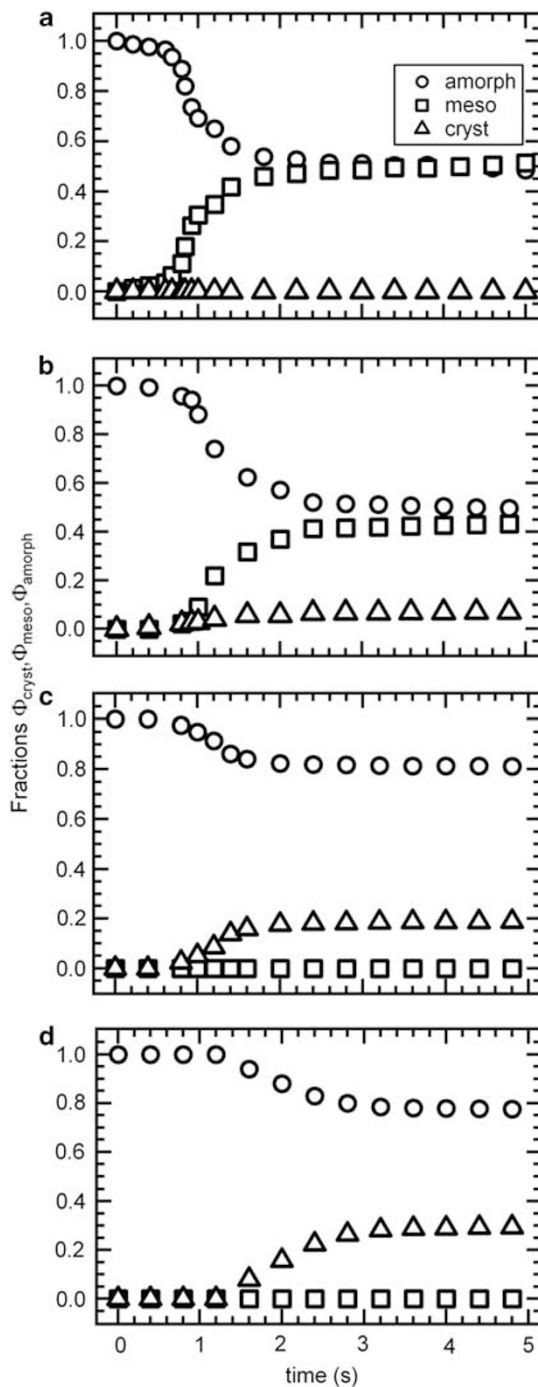


**Figure 4** Fractions of alpha-crystal,  $\Phi_{\text{crist}}$ , mesophase,  $\Phi_{\text{meso}}$  and amorphous,  $\Phi_{\text{amorph}}$  components as a function of time,  $t$ , during the rapid cooling process. The conditions in (a–d) correspond to those in Figures 2a–d, respectively.

rate is estimated under isothermal or constant cooling rate conditions. However, the cooling carried out in this experiment was considerably rapid, as shown in Figure 1, such that neither the ideal isothermal nor the constant cooling rate conditions are fulfilled. In such nonideal conditions, it is difficult to determine the proper formation rate of the mesophase. We also employed conditions defined by the differential fraction of the mesophase and the change in temperature, which corresponds to the increase in the mesophase fraction with decreasing

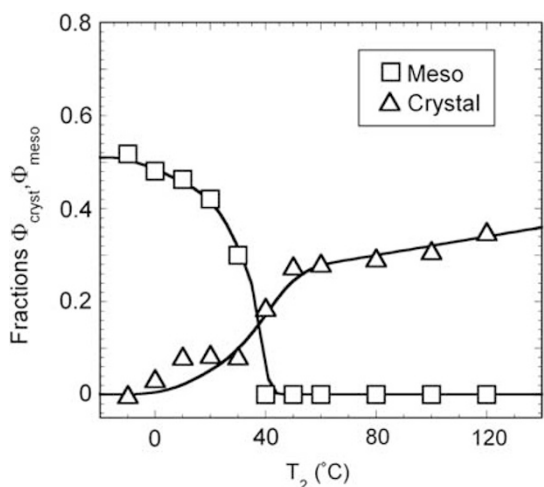


**Figure 5** Final fractions of alpha-crystal  $\Phi_{\text{cryst}}$  and mesophase  $\Phi_{\text{meso}}$  phases at the end of cooling as a function of temperature,  $T_2$ .

temperature,  $d\Phi_{\text{meso}}/(-dT)$ . This value qualitatively corresponds to a formation rate of the mesophase at each temperature. Such an apparent formation rate is obtained as follows. Referring to the  $T(t)$  curve (Figure 1),  $\Phi_{\text{meso}}(t)$  (Figure 4a) is converted into  $\Phi_{\text{meso}}(T)$ , then  $d\Phi_{\text{meso}}/(-dT)$  is obtained by differentiating  $\Phi_{\text{meso}}(T)$  by  $T$ . The results are shown as a function of  $T$  (Figure 6). The resulting curve of  $-d\Phi_{\text{meso}}/dT$  shows a monomodal distribution function. Above 40 °C, it shows no significant value. With decreasing temperature, a gradual increase can be seen, and a maximum is reached at  $\sim 10$  °C. The curve of  $-d\Phi_{\text{meso}}/dT$  then begins to decrease below 10 °C and tends to converge to zero at  $\sim -10$  °C. As will be discussed in the next section, it should be noted that the present formation rate of the mesophase of iPP was obtained along a ‘specific’ thermal path.

### Suitable kinetic paths for mesophase formation

It is often considered that a rapid quenching is essential in order to obtain the mesophase iPP without developing a crystal fraction, while too rapid quenching to a deep supercooled state vitrifies the molten iPP without forming the mesophase, as was demonstrated by an ultra-quenching technique.<sup>7,24</sup> With this in mind, we wanted to determine the suitable cooling rates and suitable quenching temperatures. As was mentioned previously, a cooling rate of  $100\text{ °C s}^{-1}$  has been a standard, but this is an estimate and is unspecific. The suitable kinetic paths for mesophase formation should be considered more specifically. The results of the ultra-fast DSC work<sup>23</sup> were obtained with constant cooling rates (Figure 2 in Gradys *et al.*<sup>23</sup>). When the cooling rate was  $<3000\text{ °C min}^{-1}$  ( $50\text{ °C s}^{-1}$ ), almost all of the heat flow was due to crystallization. In increasing the cooling rate to  $>3000\text{ °C min}^{-1}$ , the heat flow was due to the increase in mesophase formation, and the heat flow due to crystallization gradually decreased. The heat flow due to mesophase formation was at a maximum of  $9000\text{ °C min}^{-1}$  ( $150\text{ °C s}^{-1}$ ); however, at this cooling rate, crystallization still contributed significantly, and a bimodal distribution in the heat flow was observed at  $\sim 60$  and  $15$  °C for the crystal and mesophase, respectively. A suitable cooling rate for the mesophase formation could not effectively suppress crystallization. Faster cooling rates, exceeding  $9000\text{ °C min}^{-1}$ , suppressed both crystallization and mesophase formation considerably. The cooling rate that gives the fastest rate of mesophase formation does not correspond to the cooling rate that gives the slowest rate for crystallization.

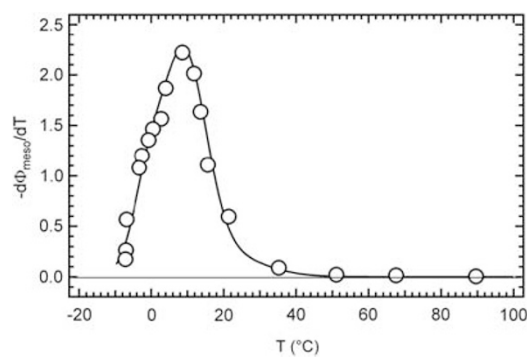


**Figure 6** The differential fraction of the mesophase of iPP and temperature change,  $-d\Phi_{\text{meso}}/dT$ , as a function of temperature,  $T$ , along a specific thermal path as shown in Figure 1. This value represents the increment of mesophase fraction with decreasing temperature,  $d\Phi_{\text{meso}}/(-dT)$  and qualitatively corresponds to the formation rate of the mesophase at each temperature.

The mesophase iPP, not including the crystal fraction, can be obtained by the empirical quenching method, that is, by dropping the sample into ice water. With empirical quenching, the initial cooling rate is very large, and the rate decreases progressively with time. With such a cooling trajectory, the cooling rate is not only large enough to suppress crystallization in the temperature range 80–90 °C, where the rate of crystallization is at a maximum,<sup>29,30</sup> but is also able to cause mesophase formation in the temperature range 10–30 °C, where its formation rate is at a maximum.<sup>29</sup> Thus, the empirical quenching method inadvertently allowed for the realization of a suitable kinetic pathway for mesophase formation. It is believed that the ideal path to obtain mesophase iPP at the maximum rate should be with isothermal annealing at  $\sim 10$ –30 °C, with a subsequent quenching at an infinitely large cooling rate.

### Mechanism of mesophase formation

The term ‘homogeneous’ is often interpreted by two ways in the relevant field. One is used to express the homogeneity of material, and the other is the homogeneity in space. To clarify, we define the former and the latter ‘materially homogeneous’ and ‘spatially homogeneous’, respectively.

On the basis of a theory by Olmsted *et al.*,<sup>31</sup> we propose a general model for the crystallization mechanism (for example, see Figure 31 in Kaji *et al.*<sup>32</sup>). The mechanism is categorized into three regions according to the supercooling depth,  $\Delta T$ , from the melting temperature,  $T_m$ . In order from small to large  $\Delta T$ , these regions are a direct crystal nucleation, binodal crystallization and spinodal crystallization. The first region is where the melt and crystals coexist in the phase diagram of the polymer melt by Olmsted, where crystal nucleation occurs directly from the melt, and classical crystal nucleation theory<sup>33</sup> seems to only be valid here. The other two regions involve phase separation between oriented (nematic) and unoriented (isotropic) phases before crystallization. In the binodal crystallization region, spherical nuclei or droplets of nematic phase are first formed in the isotropic melt and grow with time, and thereafter, crystallization is initiated inside the droplets through a smectic phase. Such a binodal or nucleation and growth (N&G) type of phase separation occurs in the metastable region of the phase diagram. In the spinodal crystallization region, a spinodal decomposition (SD) type of phase separation first occurs between the nematic and isotropic phases with a quasi periodicity when the system falls into the unstable state of the phase

diagram, and then crystallization occurs in the nematic phase part through the smectic phase. Such a smectic phase appearing midway before crystallization corresponds to the mesophase. Although the order parameter is different, this phase separation is similar to that of polymer blends.

The usual spherulites are produced from the N&G region and not from the direct crystal nucleation region where single crystals seem to form directly from the melt at extremely slow rates. In the N&G regime, spherical nuclei or droplets are produced sporadically in time and randomly in space as well as grow in size with time. Accordingly, the resulting morphology shows a spatially inhomogeneous structure consisting of randomly arranged spherical domains or polygonal domains in the final stage. As described above, the internal structure of these spherical entities or droplets in the initial stage is regarded as a nematic liquid crystal where the molecules may be oriented perpendicular to the radius of each sphere. This scheme may provide evidence for explaining the formation process of the internal structure of the spherulite (see Imai et al.<sup>34</sup>). Furthermore, in real systems, the nucleation of the nematic droplets, not the crystal nucleation, would be accelerated by impurities because nucleation assisted by impurities goes through a lower free-energy path, and the heterogeneous nucleation of droplets can occur at a smaller supercooling temperature.<sup>35</sup>

When the isotropic melt falls into the SD region, it becomes unstable; therefore, the fluctuations due to molecular orientation appear instantaneously all over the system, accompanied by a characteristic wavelength. Accordingly, the resulting morphology is likely to form a quasi-periodic structure that is spatially homogeneous on a larger scale than the characteristic wavelength. Moreover, because the driving force of the SD is very large, owing to the unstable transition at a deep supercooling, both the SD process and the crystallization that follows will not be affected by impurities. Therefore, the crystallization in the unstable state seems to occur by the materially homogeneous nucleation, even in the presence of impurities.

Figure 7 shows a series of optical micrographs of iPP during a rapid cooling process at  $T_2=10^\circ\text{C}$ . Figures 7a–d are micrographs of 0.25, 0.5, 0.75 and 1.0 s after quenching, corresponding to 125, 70, 35 and  $25^\circ\text{C}$ , respectively. In Figures 7a and b, growing spherical domains or droplets with different diameters are observed. Specifically, they should have been generated sporadically in time and randomly in space. On the other hand, as can be seen in Figure 7c, instantaneous fluctuations all over the system are observed. A Fourier transformation of the image in Figure 7c gives a broad shoulder at  $\sim 3\mu\text{m}^{-1}$  in reciprocal space, corresponding to ca  $2\mu\text{m}$  in real space. This result indicates that there exists a weak periodicity in the system. We believe this periodicity is due to the SD structure. Thus, the randomly arranged spherical domain structure and the periodic structure show the characteristics of the binodal (N&G) and SD phase separation, respectively. Both of these phase-separated, ordered regions initially assume an internal structure of a nematic phase and then convert to a smectic phase or mesophase, from which crystallization is initiated. The transformation from nematic to smectic should involve a secondary phase separation to exclude molecular entanglements in the nematic phase, which produces very small order particles or so-called nodules and amorphous regions including entanglements. This process proceeds relatively quickly, but crystallization from the smectic phase takes some time depending on the temperature and may be one reason why the mesophase is relatively stable. Another possible reason could be an increase in the glass transition temperature<sup>24</sup> with increasing mesophase fraction, which may freeze the crystallization process incompletely at the mesophase. Meanwhile, in the N&G region, which is more favorable for crystallization in iPP, the

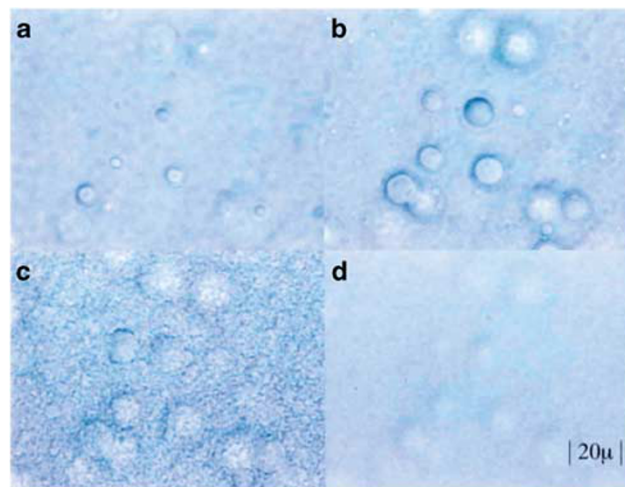


**Figure 7** Time evolution of optical micrographs immediately after molten iPP was rapidly cooled to temperature  $T_2=10^\circ\text{C}$ . (a)  $t=0.25\text{ s}$  ( $T=\text{ca } 125^\circ\text{C}$ ), (b)  $t=0.5\text{ s}$  ( $T=\text{ca } 70^\circ\text{C}$ ), (c)  $t=0.75\text{ s}$  ( $T=\text{ca } 35^\circ\text{C}$ ), (d)  $t=1.0\text{ s}$  ( $T=\text{ca } 25^\circ\text{C}$ ).

mesophase exists only transiently at the beginning of crystallization<sup>36</sup> and is therefore barely detectable by WAXD (Figures 2c and d).

We have made progress in understanding the mechanism by which the mesophase of iPP forms. Further studies will be required to fully elucidate this mechanism.

#### ACKNOWLEDGEMENTS

This work was supported by KAKENHI (Grant-in-Aid for Scientific Research) from the Ministry of Education, Culture, Sports, Science and Technology of Japan. Synchrotron radiation experiments were performed at BL45XU in SPring-8 with the approval of the Japan Synchrotron Radiation Research Institute (JASRI) (Proposal No. 2008A1526).

- Natta, G. Progress in five years of research in stereospecific polymerization. *SPE. J.* **15**, 373–382 (1959).
- Natta, G. & Corradini, P. Structure and properties of isotactic polypropylene. *Nuovo Cimento Suppl.* **15**, 40–51 (1960).
- Turner-Jones, A., Aizlewood, J. M. & Beckett, D. R. Crystalline forms of isotactic polypropylene. *Makromol. Chem.* **75**, 134–158 (1964).
- Shibayama, M., Katoh, K., Iwamoto, T., Takahashi, D. & Nomura, S. Structure of high transparent polypropylene film. *Polymer* **J.** **23**, 837–846 (1991).
- Miller, R. L. On the existence of near-range order in isotactic polypropylenes. *Polymer* **1**, 135–(1960).
- Ogawa, T., Miyaji, H. & Asai, K. Nodular structure of polypropylene. *J. Phys. Soc. Jpn.* **54**, 3668–3670 (1985).
- Hsu, C. C., Geil, P. H., Miyaji, H. & Asai, K. Structure and properties of polypropylene crystallized from the glassy state. *J. Polym. Sci., Part B: Polym. Phys.* **24**, 2379–2401 (1986).
- Zia, Q., Androsch, R., Radsch, H.-J. & Piccarolo, S. Morphology, reorganization and stability of mesomorphic nanocrystals in isotactic polypropylene. *Polymer* **47**, 8163–8172 (2006).
- Zia, Q., Radsch, H.-J. & Androsch, R. Direct analysis of annealing of nodular crystals in isotactic polypropylene by atomic force microscopy, and its correlation with calorimetric data. *Polymer* **48**, 3504–3511 (2007).
- Piccarolo, S., Saiu, M., Brucato, V. & Titomanlio, G. Crystallization of polymer melts under fast cooling. II. High-purity iPP. *J. Appl. Polym. Sci.* **46**, 625–634 (1992).
- Choi, C.-H. & White, J. L. Correlation and modeling of the occurrence of different crystalline forms of isotactic polypropylene as a function of cooling rate and uniaxial stress in thin and thick parts. *Polym. Eng. Sci.* **40**, 645–655 (2000).
- Brucato, V., Piccarolo, S. & Carrubba, V. L. An experimental methodology to study polymer crystallization under processing conditions. The influence of high cooling rates. *Chem. Eng. Sci.* **57**, 4129–4143 (2002).
- Coccorullo, I., Pantani, R. & Titomanlio, G. Crystallization kinetics and solidified structure in iPP under high cooling rates. *Polymer* **44**, 307–318 (2003).
- Konishi, T., Nishida, K., Kanaya, T. & Kaji, K. Effect of isotacticity on formation of mesomorphic phase of isotactic polypropylene. *Macromolecules* **38**, 8749–8754 (2005).

- 15 Li, L. & de Jeu, W. H. Shear-induced smectic ordering and crystallisation of isotactic polypropylene. *Faraday Discuss.* **128**, 299–319 (2005).
- 16 Androsch, R. & Wunderlich, B. Reversible crystallization and melting at the lateral surface of isotactic polypropylene crystals. *Macromolecules* **34**, 5950–5960 (2001).
- 17 Wang, Z. G., Hsiao, B. S., Srinivas, S., Brown, G. M., Tsou, A. H., Cheng, S. Z. D. & Stein, R. S. Phase transformation in quenched mesomorphic isotactic polypropylene. *Polymer* **42**, 7561–7566 (2001).
- 18 Nishida, K., Konishi, T., Kanaya, T. & Kaji, K. Novel morphology of isotactic polypropylene crystal generated by a rapid temperature jump method. *Polymer* **45**, 1433–1437 (2004).
- 19 Konishi, T., Nishida, K. & Kanaya, T. Crystallization of isotactic polypropylene from prequenched mesomorphic phase. *Macromolecules* **39**, 8035–8040 (2006).
- 20 Zhao, J., Qiu, J., Niu, Y. & Wang, Z. Evolutions of morphology and crystalline ordering upon annealing of quenched isotactic polypropylene. *J. Polym. Sci., Part B: Polym. Phys.* **47**, 1703–1712 (2009).
- 21 Asakawa, H., Nishida, K., Matsuba, G., Kanaya, T. & Ogawa, H. Crystallization of isotactic polypropylene from mesomorphic phase: a constant heating rate study. *J. Phys.: Conf. Ser.* **272**: [012024-1]–[012024-4] (2011).
- 22 Wu, Z. Q., Dann, V. L., Cheng, S. Z. D. & Wunderlich, B. Fast DSC applied to the crystallization of polypropylene. *J. Therm. Anal.* **34**, 105–114 (1988).
- 23 Grady, A., Sajkewicz, P., Minakov, A. A., Adamovsky, S., Schick, C., Hashimoto, T. & Saijo, K. Crystallization of polypropylene at various cooling rates. *Mater. Sci. Eng. A* **413–414**, 442–446 (2005).
- 24 Miyamoto, Y., Fukao, K., Yoshida, T., Tsurutani, N. & Miyaji, H. Structure formation of isotactic polypropylene from the glass. *J. Phys. Soc. Jpn.* **69**, 1735–1740 (2000).
- 25 Cavallo, D., Azzurri, F., Floris, R., Alfonso, G.C., Balzano, L. & Peters, G. W. Continuous cooling curves diagrams of propene/ethylene random copolymers. The role of ethylene counits in mesophase development. *Macromolecules* **43**, 2890–2896 (2010).
- 26 Cavallo, D., Portale, G., Balzano, L., Azzurri, F., Bras, W., Peters, G. W. & Alfonso, G. C. Real-time WAXD detection of mesophase development during quenching of propene/ethylene copolymers. *Macromolecules* **43**, 10208–10212 (2010).
- 27 Fujisawa, T., Inoue, K., Oka, T., Iwamoto, H., Uruga, T., Kumasaka, T., Inoko, Y., Yagi, N., Yamamoto, M. & Ueki, T. Small-angle X-ray scattering station at the SPring-8 RIKEN beamline. *J. Appl. Cryst.* **33**, 797–800 (2000).
- 28 Nishida, K. Rapid temperature jump stage for optical microscope. *Proc. Polymer Processing Soc.* S17–631 (2008).
- 29 Silvestre, C., Cimmino, S., Duraccio, D. & Schick, C. Isothermal crystallization of isotactic poly(propylene) studied by superfast calorimetry. *Macromol. Rapid Commun.* **28**, 875–881 (2007).
- 30 Nakamura, K., Shimizu, S., Umamoto, S., Thierry, A., Lotz, B. & Okui, N. Temperature dependence of crystal growth rate for a and b forms of isotactic polypropylene. *Polym. J.* **40**, 915–922 (2008).
- 31 Olmsted, P. D., Poon, W. C. K., McLeish, T. C. B., Terrill, N. J. & Ryan, A. J. Spinodal-assisted crystallization in polymer melts. *Phys. Rev. Lett.* **81**, 373–376 (1998).
- 32 Kaji, K., Nishida, K., Kanaya, T., Matsuba, G., Konishi, T. & Imai, M. Spinodal crystallization of polymers: crystallization from the unstable melt. *Adv. Polym. Sci.* **191**, 187–240 (2005).
- 33 Turnbull, D. & Fisher, J. C. Rate of nucleation in condensed systems. *J. Chem. Phys.* **17**, 71–73 (1949).
- 34 Imai, M. & Kaji, K. Polymer crystallization from the metastable melt: the formation mechanism of spherulites. *Polymer* **47**, 5544–5554 (2006).
- 35 Janeschitz-Kriegl, H. Conditions of nucleation in crystallizable polymers: reconnaissance of positions - a critical evaluation. *Colloid. Polym. Sci.* **275**, 1121–1135 (1997).
- 36 Strobl, G. From the melt via mesomorphic and granular crystalline layers to lamellar crystallites: a major route followed in polymer crystallization? *Eur. Phys. J. J.* **3**, 165–183 (2000).